Electrochimica Acta 232 (2017) 203–214

Contents lists available at ScienceDirect

Electrochimica Acta

journal homepage: www.elsevier.com/locate/electacta

A mass transfer based variable porosity model with particle radius change for a Lithium-ion battery

T.R. Ashwin[a,b], A. McGordon[a], P.A. Jennings[a,*]

[a] WMG, University of Warwick
[b] Centre for Scientific Computing, University of Warwick, Coventry. CV4 7AL. U.K.

ARTICLE INFO

Article history:
Received 21 November 2016
Received in revised form 21 February 2017
Accepted 22 February 2017

Keywords:
Lithium-ion battery
P2D model
Variable Porosity
Mass transfer

ABSTRACT

Micro pore-clogging in the electrodes due to SEI growth and other side reactions can cause adverse effects on the performance of a Lithium-ion battery. The fundamental problem of volume fraction variation and particle radius change during the charge-discharge process in a lithium-ion battery is modelled in this paper with the help of mass transfer based formulation and demonstrated on a battery with $LiCoO_2$ chemistry. The model can handle the volume fraction change due to intercalation reaction, solvent reduction side reaction and the electrolyte density change due to side reaction contamination in the battery. The entire calculation presented in this paper models particle radius and volume fraction together and therefore gives greater accuracy in calculating the volume-specific-area of the reacting particles which is an important parameter controlling the Butler-Volmer kinetics. The mass deposit on the electrode (or loss of lithium) gives an indication of the amount of pre-lithiation required to maintain cell performance while the amount of mass deposited on the SEI helps to decide the safe operating condition for which the clogging of pores and capacity fade will be minimal. Moreover the model presented in this paper has wide applicability in analysing the stress development inside the battery due to irreversible porous filling.

1. Introduction

A Pseudo Two Dimensional (P2D) model offers flexibility in solving the interlinked chemical governing equations of a Lithium-ion battery based on concentrated solution theory [1,2]. The volume fraction change during charging and discharging, and the Solid Electrolyte Interphase (SEI) grows over the particles forming a porous film, which is responsible for the lithium loss and voltage drop [3]. The pores expand and contract during normal charging and discharging imposing stress on the interior layers of the battery; [4] suggests that the stress could be of significant level and even could damage the particle near the separator. A higher stress development can be also observed in batteries with Silicon anode material [5,6]. The capacity fade of the battery can get accelerated by constriction of pores in the electrode, due to side reactions. SEI build up increases the internal resistance of the battery leading to excessive heat generation while charging and discharging. The fact that excessive heat generation accelerates the SEI growth has been already proven by researchers and therefore this effect can lead to accelerated power fade and capacity fade.Parametric studies with different heat transfer coefficient and the resulting SEI growth can be found in Ashwin *et al.* [7] for a single cell battery and for a battery pack in Ashwin *et al.* [8]. Thus the intercalation and other side reactions need to be captured accurately to model the volume fraction change. Moreover, many of the empirical relations used in earlier models can be eliminated by including a time varying volume fraction. The motivation for this paper is to develop a more fundamental model which predicts the mass transfer across the anode-separator-cathode boundaries by measuring the Li^+ concentration in the electrolyte within the framework of a P2D model.

Han *et al.* [9] modelled the intercalation process with phase field variables which is accurate and allows simpler tracking of phase boundaries than Fick's equation. There were other studies such as Singh *et al.* [10] who developed a continuum based theory for the intercalation process in a single crystal rechargeable battery. Another model was presented by Teixidor *et al.* [11] for the analysis of fractal-like electrodes for lithium-ion batteries and this study proved an optimal electrode configuration of the fractals for electrochemical energy storage. Thus, most of the intercalation studies are either on a crystalline battery or on flow batteries. There have

* Corresponding author.
E-mail addresses: A.T.Rajan@warwick.ac.uk (T.R. Ashwin), A.McGordon@warwick.ac.uk (A. McGordon), Paul.Jennings@warwick.ac.uk (P.A. Jennings).

http://dx.doi.org/10.1016/j.electacta.2017.02.129

Nmenclature

a	Active surface area per unit volume (cm^{-1})
A	Electrode plate area (cm^2)
c	Volume-averaged concentration ($mol\,cm^{-3}$)
D	Diffusion coefficient ($cm^2\,s^{-1}$)
F	Faraday constant, 96487 $C\,mol^{-1}$
i_o	Exchange current density for intercalation reaction ($A\,cm^{-2}$)
i_{os}	Exchange current density for solvent reduction reaction ($A\,cm^{-2}$)
I_{app}	Applied current (A)
J_1	Reaction current for intercalation reaction ($A\,cm^{-3}$)
J_s	Reaction current for solvent reduction reaction ($A\,cm^{-3}$)
K	Number of spherical particles
L	Cell width (cm)
M, $\hat{M}$	Initial mass, Mass at a time step during battery operation (kg)
Q	Cycle number
r	Radial coordinate (cm)
R	Universal gas constant, 8.3143 ($J\,mol^{-1}\,K^{-1}$)
ΔX	Length of the control volume (cm)
t	Time (s)
t_+^0	Transference number
V	Cell voltage (V)
$\bar{Vl}$	Volume (cm^3)
$\hat{V}$	Molar mass (g/mol)

Greek Symbols

ρ	Density ($kg\,cm^{-3}$)
α_a, α_c	Charge-transfer coefficient
δ	Thickness (cm)
ϵ	Volume fraction of domain
Λ	Particle radius (cm)
η	Over potential (V)
κ	Conductivity of electrolyte ($S\,cm^{-1}$)
κ_D	Diffusivity ($A\,cm^{-1}$)
σ	Solid phase conductivity ($S\,cm^{-1}$)
ϕ	Volume averaged potential (V)
χ	Volumetric mass of porous media ($kg\,cm^{-3}$)

Superscript and subscript

avg	average
cv	Control volume
eff	Effective
e, *s*, *f*	Electrolyte, solid and binder
SEI	Solid Electrolyte Interphase
n, *p*, *sep*	Negative, positive and separator
t	time step

List of Acronyms

P2D	Pseudo Two Dimension
SEI	Solid Electrolyte Interphase
SoC	State of Charge

been many studies on SEI growth due to side reactions, but very few studies quantified mass deposition due to intercalation process for example Pinson and Bazant [12].

The existing models have helped to understand the intercalation process and the growth of chemical deposition in a battery more clearly. However,there are very few modelling contributions on the side reactions and mass deposition due to SEI growth. One of the novel contributions to model capacity fade in a battery is by Ramadass [13] *et al.* who developed a capacity fade model under the assumption of a continuous solvent reduction side reaction. This model helped researchers to quantify the resistance increase due to SEI growth and the resulting change in voltage-current characteristics. The SEI growth has been studied by several other researchers, for example Radvanyi *et al.* [14] who used an impedance spectroscopy method to investigate the instability of the SEI on the surface of the silicon particles. A general model for the discharge deposit formation is studied by Wang [15] for a lithium-air battery, who found that the discharge products precipitate at reaction sites increasing the particle radius. The present work is inspired by this study to develop a variable volume fraction, variable particle radius model for a lithium-ion battery within the framework of a P2D model.

The internal stress imposed by the two chemical reactions of intercalation and the SEI deposition, is studied by few researchers. The modelling study by Renganathan *et al.* [4] shows that stress generation caused by phase transformation could be significant. The influence of external stress was investigated by few other researchers for example, Gao *et al.* [16] studied the yield stress of a Li_xSn battery material as the change of charge states. A detailed study on the effect of external stress on batteries can be found in Kim [17] who identified and quantified key sources of mechanical stresses including manufacturing-induced loads, thermal loads, kinetic loads and structural loads and the findings were verified using molecular dynamics simulations. The stress level is significantly large in Silicon anode batteries and a detailed study is presented by Beattie *et al.* [5,6]. A two-phase transition model has been developed by Li *et al.* [18] during galvanostatic charging and discharging for a lithium iron phosphate (LFP) battery. The lithiation and delithiation in LFP particles is approximated using a shrinking core with a moving interface between the two phases. However, to capture these effects accurately, the volume fraction change also should be modeled from fundamental chemical reactions.

There were attempts to simplify the chemical reactions in a battery using correlations or by using theoretical parameters. A correlation based electrochemical model for a graphite electrode was presented in Novak *et al.* [19]. The results show that by adjusting the volume fraction, the electrochemical performance of graphite electrodes could be improved. The present work is aiming to remove the correlation based approach used by models like Novak *et al.* and thereby modelling the chemical reactions from fundamental kinetics.

Later, Gu *et al.* [20] and Sikha *et al.* [21] modelled the change in volume fraction due to irreversible parasitic side reactions. In all of the referensed models, the volume change was linked to the partial molar volume of the reacting species, which is difficult to measure. Moreover, this model needs information about SEI growth to calculate irreversible porous filling therefore the research community is looking forward to overcoming this limitation. Moreover, there can be variations in molar concentration due to side reaction contamination [22]. Another notable attempt was made by Yoo *et al.* [23] who used a moving boundary to capture the volume change in a Lithium-air battery and Garrick *et al.* [24] who correlated volume fraction change to stress development. Ashwin *et al.* [7,8] developed a variable volume fraction model linked to capacity fading and distributed thermal model. This model was successful in predicting different amounts of micro-pore plugging but the volume fraction variation was again based on partial molar volume.

The above mentioned studies proved that the property variation in an electrolyte has severe implications on the performance of a battery. Unfortunately, to the best of authors knowledge, there were no theoretical investigations to quantify the density change or property change in an electrolyte of a lithium-ion battery caused by various side reactions. There are several experimental

Table 1
Mass based parameters calculated in this model

	Negative electrode	Separator	Positive electrode
Initial mass calculation of the battery(Constant)			
Initial total mass	Mi_n	Mi_{sep}	Mi_p
Initial electrolyte mass	$Mi_{e,n}$	$Mi_{e,sep}$	$Mi_{e,p}$
Initial solid mass	$Mi_{s,n}$	No solid mass	$Mi_{s,p}$
Initial binder/filler mass	$Mi_{f,n}$	$Mi_{f,sep}$	$Mi_{f,p}$
Instantaneous mass calculation			
Total instantaneous mass	$\tilde{M}_n$	$\tilde{M}_{sep}$	$\tilde{M}_p$
Electrolyte instantaneous mass	$\tilde{M}_{e,n}$	$\tilde{M}_{e,sep}$	$\tilde{M}_{e,p}$
Solid instantaneous mass	$\tilde{M}_{s,n}$	No solid mass	$\tilde{M}_{s,p}$
Mass deposited during change &discharge			
Total deposited/liberated mass at time t	$\Delta M_{n,t}$		$\Delta M_{p,t}$

investigations which need support from the modelling community to accurately predict the battery performance variation with electrolyte contamination and micro-pore plugging. Some experimental examples are by Hein and Latz [25] who investigated the degradation process due to deposition of metallic lithium on the surface of active particles and Xu *et al.* [26] who investigated the cycliability of lithium metal batteries by adding potassium ion to the electrolyte.

The model presented in this work reduces the complexity in capturing the volume fraction and radius changes and the experimental measurements reduces to the determination of density and molar mass of the reactants and deposit which avoids the need to determine the partial molar concentration. Moreover, the present model solves only algebraic equations which do not add computational load to the system. A novel approach of SEI deposition is adopted in this work to monitor the average lithium-ion concentration of the electrolyte after each cycle and the difference is then added to the solid mass in the negative electrode as the SEI thickness. So far, in electrochemical modelling, the SEI is treated only as an internal resistance causing capacity fade. Also, the phenomenon of micro-pore plugging is believed to be due to SEI filling and side reactions. This paper puts forward another perspective which couples SEI resistance and mass deposition together. The radius-volume fraction calculation can bring more accuracy for P2D model predictions by improving the accuracy of volume-specific-area prediction for chemical reactions. The amount of pre-lithiation is quantified in terms of mass deposit for the first time. The mass deposit contributing to the growth of SEI is quantified which will help to decide the amount of pore-plugging and the particle cracking at different operating conditions. This work also accounts for the change in density of the electrolyte which can represent the contamination of the electrolyte due to side reactions, for the first time. A FORTRAN program is developed to support the mass conservation equations using the mathematical framework of P2D model equations. Thus, this model will be able to support a wide range of experimental investigations since stress development, particle cracking and lithium plating occur during different operating phases of the battery.

The paper is structured as follows: Section 2 presents the governing equations for this model; the supporting Newman's model equations and the boundary conditions are presented in Table 3. The solution methodology is listed in Section 3 while the results and discussion are presented in Section 4. The applications of the model and the novel contributions are presented in Section 5 followed by a conclusion in Section 6.

2. Model development & governing equations

This section lists the necessary governing equations for the calculation of mass deposition in the lithium ion battery. This is strongly based on the principle of mass conservation and also on the assumption that the total mass of the battery remains the same for a fresh cell and an aged cell; only energy can be transferred across the boundaries. The mass accumulation and SEI layer formation is only treated as a mass displacement due to chemical reactions. The term "mass deposit" in this manuscript refers to the mass due to intercalation or SEI formation.

The negative composite electrode (Fig. 1) is made of active material of LiC_6 and the positive electrode is made with metal oxide active material such as $LiCoO_2$ and the salt is $LiPF_6$. During charging, positive Lithium ions from the positive electrode diffuse to the negative electrode. However in practice the Solid Electrolyte Interphase (SEI) layer consumes some of these lithium ions contributing to the thickening of the layer, predominantly at the negative electrode [13].

At the negative electrode:

$$x\,Li\,C_6 \underset{charge}{\overset{discharge}{\rightleftarrows}} x\quad C_6 + x\,e^- + x\,Li^+$$

At the positive electrode:

$$CoO_2 + y\,Li^+ + y\,e^- \underset{charge}{\overset{discharge}{\rightleftarrows}} Li_yCoO_2$$

The initial and instantaneous mass calculated is presented in Table 1.

2.1. Initial mass calculation of the battery

The initial volumetric mass (χ) of a control volume can be calculated from the initial volume fraction values of each electrode as follows. The actual values used in this work are given in Table 2.

$$\chi_t = \chi_n + \chi_{sep} + \chi_p$$

where

$$\chi_{n,sep,p} = \epsilon_e \rho_e + \epsilon_s \rho_s + \epsilon_f \rho_f$$

The subscript s refers to the reacting solid mass in anode and cathode which is capable of taking part in intercalation and side reactions. Henceforth, all the mass based parameters represented in Table 1 with subscript s or the notation "solid mass" refers to the reacting mass in this manuscript. The subscript f represents filler material other than solid and the electrolyte; otherwise however he binder material used to hold the solid mass together. The filler is an inert mass which will not take part in chemical reactions. Henceforth, all the mass based parameters with subscript f or the notation "filler" refers to the non-reacting mass in this manuscript. There is non-reacting solid mass in the separator therefore $\epsilon_s \rho_s$

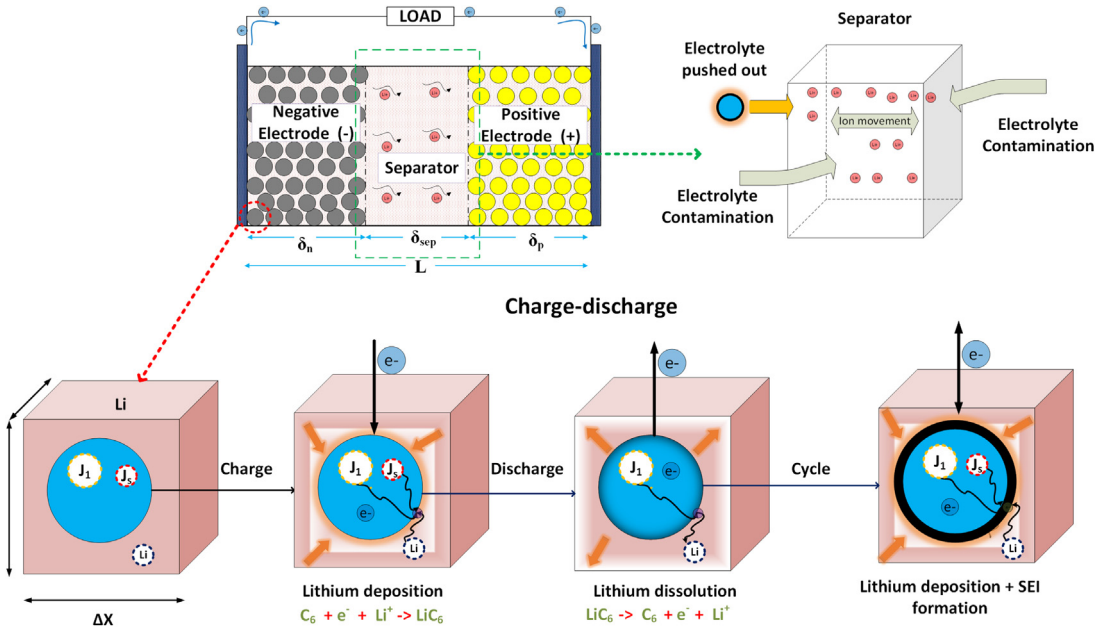

Fig. 1. Description of the mass balance model: Layout of the battery

Table 2
Electro-chemical parameters of 6Ah battery used to implement mass transfer model

	Negative Electrode	Separator	Positive Electrode
Thickness, δ (cm)	50×10^{-4}	25.4×10^{-4}	36.4×10^{-4}
Particle radius, Λ_s (cm) [1]	1×10^{-4}		1×10^{-4}
Active material volume fraction ϵ_s [1]	0.580		0.500
Electrolyte phase volume fraction ϵ_e [1]	0.332	0.5	0.330
Maximum solid phase concentration $c_{s,max}$ (mol cm^{-3})	16.1×10^{-3}		23.9×10^{-3}
Stoichiometry at 0% SOC	0.126		0.936
Stoichiometry at 100% SOC	0.676		0.442
Average electrolyte concentration c_e (mol cm^{-3})	1.2×10^{-3}	1.2×10^{-3}	1.2×10^{-3}
Exchange current density (i_o) (A cm^{-3})	3.6×10^{-3}		2.6×10^{-3}
Charge-transfer coefficients α_a, α_c	0.5, 0.5		0.5, 0.5
SEI layer film resistance, Ω_{SEI} (Ω cm^2)	100		100
Solid phase Li diffusion coefficient, D_s (cm^2 s^{-1})	2.0×10^{-12}		3.7×10^{-12}
Solid phase conductivity, σ (S cm^{-1})	1.0		0.1
Electrolyte phase Li$^+$ diffusion coefficient, D_e (cm^2 s^{-1})	2.6×10^{-6}	2.6×10^{-6}	2.6×10^{-6}
Bruggeman porosity exponent, p	1.5	1.5	1.5
Electrolyte activity coefficient, $f^{\pm}$	1.0	1.0	1.0
Li$^+$ transference number, t_+^0	0.363	0.363	0.363
Density of electrolyte ρ_e (kg cm^{-3})	1123.0×10^{-6}	(1123.0×10^{-6}) [1]	1123.0×10^{-6}
Density of solid phase ρ_s (kg cm^{-3})	1347.3×10^{-6}		2328.5×10^{-6}
Reference voltage U_{ref} (V)	0		0
Molecular weight M_{SEI} (kg mol^{-1})	7.3×10^4		
Density of SEI Layer ρ_{SEI} (kg cm^{-3})	2.1×10^{-3}		
Side reaction exchange current density i_{os} [1] (A cm^{-3})	1.5×10^{-12}		
Conductivity of SEI Layer κ_p (S cm^{-1})	1×10^{-4}		

[1] Initial values; variable according to calculations presented.

contribution remains zero. Thus the initial total mass of the battery can be calculated using the following expression at each electrode,

$$Mi_{n,sep,p} = \sum_{n=1}^{N_{cv}} \chi_t \Delta \bar{V} l_{cv} \tag{1}$$

where N_{cv} is the number of control volumes in each electrode (N_n, N_{sep},N_p) and $\Delta \bar{V} l_{cv}$ corresponds to the volume of each control volume. $\Delta \bar{V} l_{cv}$ is calculated as $A_{n,p} \Delta X$, where $A_{n,p}$ is the area of each electrode and ΔX is the length of each control volume. Thus $\sum_{n=1}^{N_{cv}} \Delta X$ is equal to the length of the electrodes (δ).

The initial mass of negative electrode (Mi_n), positive electrode(Mi_p), separator (Mi_{sep}) and the total initial mass (Mi_t) of the battery must be calculated before any electro-chemical reactions and the aforementioned values remain constant throughout the battery life. The P2D model assumes that the electrodes are filled with spherical particles [2]. The number of spherical particles in a battery remains constant.

Thus the solid mass of each electrode is given by

$$Mi_s = \underbrace{\sum_{n=1}^{N_n} \epsilon_s \rho_s \Delta \bar{V} l_n}_{Mi_{s,n}} + \underbrace{\sum_{n=1}^{N_p} \epsilon_s \rho_s \Delta \bar{V} l_p}_{Mi_{s,p}} \tag{2}$$

The first part of the summation term represents the solid mass of the negative electrode ($Mi_{s,n}$) whereas the second part represents the solid mass of positive electrode ($Mi_{s,p}$).

Table 3
Newman model equations

	Governing equations	Boundary conditions
Conservation of charge		
Electrolyte phase	$\nabla.(\kappa^{eff}\nabla\phi_e)+\nabla.(\kappa_D^{eff}\nabla In(c_e)+J_1+J_s=0$	$\frac{\partial\phi_e}{\partial x}\|_{x=0}=\frac{\partial\phi_e}{\partial x}\|_{x=L}=0$
Solid Phase	$\nabla.(\sigma_{eff}\nabla\phi_s)=(J_1+J_s)$	$\frac{\partial\phi_s}{\partial x}\|_{x=\delta^+}=\frac{\partial\phi_s}{\partial x}\|_{x=\delta^+}=0-\sigma_{s,n}^{eff}\frac{\partial\phi_s}{\partial x}\|_{x=0}=\frac{-I_{app}}{A_n}=\sigma_{s,p}^{eff}\frac{\partial\phi_s}{\partial x}\|_{x=L}=\frac{I_{app}}{A_p}$
Conservation of lithium		
Electrolyte phase	$\frac{\partial}{\partial t}(\epsilon_e c_e)=\nabla.(D_{e,eff}\nabla c_e)+\frac{1-t_0^+}{F}(J_s+J_1)$	$\frac{\partial c_e}{\partial x}\|_{x=0}=0,\quad\frac{\partial c_e}{\partial x}\|_{x=L}=0$
Solid Phase	$\frac{\partial}{\partial t}c_s=\frac{D_s}{r^2}\frac{\partial}{\partial r}\left(r^2\frac{\partial}{\partial r}c_s\right)$	$\frac{\partial c_s}{\partial r}\|_{r=0}=0,\frac{\partial c_s}{\partial r}\|_{r=R_s}=\frac{-J_1}{a_s F}$
Kinetics		
Electrochemical reaction rate	$J_1=a_{n,p}i_o\left\{\exp\left(\frac{\alpha_{n,p}F\eta}{RT}\right)-\exp\left(-\frac{\alpha_{n,p}F\eta}{RT}\right)\right\}$	
Exchange current density	$i_0=Fk_e(c_e)^{\alpha a}(c_s^{\max}-c_{s,e})^{\alpha a}(c_{s,e})^{\alpha c}$	
SEI reaction current density	$J_s=-a_n i_{os}e^{(-\alpha_c F\eta_{SEI})}$	
Thickness of the SEI layer	$\frac{\partial\delta_{SEI}}{\partial t}=\frac{J_s M_{SEI}}{F\rho_{SEI}a_n}$	
Overpotential for the SEI reaction	$\eta_{SEI}=\phi_s-\phi_e-U_{ref}-J\frac{R_{SEI}}{a_s}$	
Overpotential for the negative electrode	$\eta_n=\phi_s-\phi_e-U-\frac{R_{SEI}}{a_s}J$	
Overpotential for the positive electrode	$\eta_p=\phi_s-\phi_e-U$	

2.2. The number of spherical particles in the battery

The model assumes that the electrodes are filled with spherical particles of volume $4\pi\Lambda^3/3$. The density of the solid phase is taken from the manufacturer specification of the battery. The total mass of spherical particles must be equal to the initial solid mass of the electrode, $Mi_{s(n,p)}$. The number of solid spherical particles in the separator is taken as zero.

The number of spherical particles (K) in the negative and positive electrode of the battery is calculated from the following equation.

$$K_{n,p}=\frac{3}{4}\frac{Mi_{s(n,p)}}{\pi\Lambda^3\rho_s} \tag{3}$$

2.3. Mass deposition due to SEI formation

The solvent reduction reaction current density (J_s) reduces the intercalaction reaction current density (J), therefore introducing a reduction in current density on the system of equations to capture ageing. The reduction in Li^+ concentration over subsequent cycles is taken as the SEI deposition over the negative electrode. The electrolyte concentration is averaged in the whole battery; negative electrode, separator and positive electrode to find the concentration depreciation. This model correlates the mass change due to SEI as follows:

$$\Delta M_{SEI}|_Q=\left[c_{avg,e}|_Q-c_{avg,e}|_{Q-1}\right]A_n\delta_n\epsilon_e\hat{V} \tag{4}$$

where the $\hat{V}$ is the molar mass of Li^+.

2.4. Mass balance during charging and discharging

The model assumes that the rate of change of Li^+ ions in the electrolyte is proportional to the mass coming out of, or going into, the solid particle in each electrode. Thus the amount of mass intercalated on to the solid particle at a particular time step in the negative electrode is given by:

$$\Delta M_{n,t}=\sum_{n=1}^{N_n}\left(c_e^t-c_e^{t-1}\right)A_n\Delta X\epsilon_e\hat{V} \tag{5}$$

The value of molar mass ($\hat{V}$) in Eq. (5) must be properly adjusted to capture the mass deposit due to other side reactions such as dissociation, temperature decomposition etc. in the battery [3]. However, in this work, the value is limited only to Lithium deposition. The Li^+ ions in the electrolyte intercalate on the graphite electrode during charging forming LiC_6 and therefore increasing the stoichiometry of the negative electrode. The reverse reaction occurs during discharge, where the Li^+ ions liberated from negative electrode are consumed at the positive electrode forming the corresponding salt (or chemical). The value of $\Delta M_{n,t}$ will be negative during charging and positive during discharge. The mass removal from the electrolyte appears in the solid phase as mass deposition.

Thus the instantaneous mass change at negative electrode is given by

$$\tilde{M}_n=Mi_{s,n}\pm\Delta M_{n,t}+\Delta M_{SEI} \tag{6}$$

Where $+\Delta M_{n,t}$ gets deposited in the negative electrode due to intercalation of Li^+ forming LiC_6 while charging and $-\Delta M_{n,t}$ gets removed during discharge forming Li^+ and C_6. The last term, ΔM_{SEI}, is the irreversible mass deposited due to SEI formation which is described in section 2.3.

The amount of mass deposited or removed from the positive electrode is given by:

$$\Delta M_{p,t}=\sum_{n=1}^{N_p}\left(c_e^t-c_e^{t-1}\right)A_p\Delta X\epsilon_e\hat{V} \tag{7}$$

The instantaneous mass at the positive electrode is given by:

$$\tilde{M}_p=Mi_{s,p}\mp\Delta M_{p,t} \tag{8}$$

The model assumes that $\Delta M_{p,t}$ is removed from the positive electrode during charging due to the formation of Li^+ and CoO_2 while $\Delta M_{p,t}$ is deposited on to the positive electrode due to the formation of $LiCoO_2$. The model assumes that there is no SEI formation on the positive electrode. The Eqs. (6–8) must be modified to incorporate the different ageing mechanisms listed in Vetter [3], once the mathematical treatment is available.

2.5. Density change in the separator

The analysis of Lithium-ion batteries with graphitic carbon anodes for prolonged cycling shows that there is a change in electrolyte properties with cycling [27]; more references can be found in a recent work by Scheers *et al.* [28]. Thus, it is evident that the solvent reduction side reaction influences the property of the electrolyte. These effects are included in Section 2.4 with an assumption that the decrease in Lithium concentration with cycling is deposited over the anode as the SEI layer.

Ideally, the generation and consumption of ions in the battery remains the same during charging or discharging. The mass (ions) liberated at the positive electrode during charge will be consumed at the negative electrode. Thus, the generation and consumption of ions in the battery remains the same during charging or discharging. There could however be an imbalance in the mass equilibrium

due to a difference in reaction rates on both electrodes; the SEI build-up can also contribute towards this. Also the increase in particle radius in the negative electrode can push out electrolyte into the separator region. This effect did not have to be taken care of in a conventional P2D model since there is no mass transfer from the electrolyte to the solid particle or there is no mass balance check at each time instant which is a simplification. The SEI layer will only contribute to the resistance increase proportional to the increase in SEI thickness δ calculated using equations listed in Table 3. Otherwise there is no check to assure that the mass deposited on to the solid particle due to SEI thickness δ is removed from the electrolyte. Also the volume increase due to SEI will not affect the conventional P2D model in any way. This paper is an effort to overcome these deficiencies of a P2D model. Both these effects have been accounted for in the present model. Mathematically, this can put additional constraint that there is no mass generation inside the battery or the density should be altered to match this. The property changes due to SEI formation, the change in property of the electrolyte, collectively due to all the above reactions is reflected as density variation since this model is based on mass balance.

The present model calculates the mass imbalance as an accumulation in the separator region which contributes towards the increase in the density of the electrolyte in the separator region. The mass imbalance (accumulation) in the separator can be calculated by subtracting the instantaneous mass of the battery from total initial mass of the battery. Thus the electrolyte mass in the separator is re-calculated to satisfy the mass conservation as:

$$\tilde{M}_{e,sep} = \underbrace{\left(Mi_n + Mi_p + Mi_{sep}\right)}_{\text{Initial mass of the battery}} - \underbrace{\left(\tilde{M}_n + \tilde{M}_p + Mi_{f,sep}\right)}_{\text{Instantaneous mass}}$$

Where $Mi_{f,sep}$ is the filler or binder mass in the separator which does not change during chemical reactions. The $\tilde{M}_{e,sep}$ gives the mass of the electrolyte in the separator region to satisfy mass conservation.

Thus the density of electrolyte in the separator is recalculated as:

$$\rho_{e,sep} = \tilde{M}_{e,sep}/A\,L_{sep}\,\epsilon_{e,sep} \tag{9}$$

where $\epsilon_{e,sep}$ is the volume fraction of electrolyte in the separator which has to remain constant since the filler volume fraction is fixed to 0.5 and therefore the electrolyte volume fraction is 0.5 in this calculation. In fact, the density variation or property change of battery is reflected in all three regions of the battery; anode, cathode and the separator. In this model the density variation is limited only to the separator to make the mathematical model computationally less expensive.

2.6. Particle radius calculation during charging and discharging

The above updated mass is distributed equally in the electrodes on to the fixed number of particles ($K_{n,p}$) calculated at the start. The local current density variations are neglected in this calculation assuming electrode homogeneity.

The radius of the particle during charging and discharging is given by

$$\Lambda^t_{n,p} = \sqrt[3]{\frac{\tilde{M}^t_{n,p}}{\frac{4}{3}\,\pi\,\rho_s\,K_{n,p}}} \tag{10}$$

where $K_{n,p}$ is from Eq. (3). The unintercalated density and intercalated density is approximated to be the same in this model, considering the fact that P2D model is formulated assuming thermodynamic equilibrium at every time step. Therefore the battery has to satisfy thermal, chemical and mechanical equilibrium at each instance of operation and separate state calculation of density is therefore impossible.

2.7. Volume fraction calculation during charging and discharging

The mass accumulated during charging, and liberated during discharging, at each electrode, contributes to the volume fraction change. As already mentioned, the number of particles in each electrode remains constant. The radius of the particle gets updated at each time step to account for the intercalation reaction. Thus, with a new radius, the new particle volume is given by $4\pi(\Lambda^t_{n,p})^3/3$. The total solid mass contributed by the solid particle should match the instantaneous solid mass of the whole electrode ($\tilde{M}_{n,p}$) calculated at that instant. Thus the mass of the electrode is given by:

$$\tilde{M}_{n,p} = A_{n,p}\,L_{n,p}\,\rho_s\,\epsilon_s$$

The volume fraction of the electrode is calculated as a bulk value. The node to node volume fraction change is neglected in this model, assuming that the current density variation is negligible in the electrode [2].

$$\epsilon^t_{s(n,p)} = \frac{4}{3}\frac{\pi(\Lambda^t_{n,p})^3 K_{n,p}}{A_{n,p}L_{n,p}} \tag{11}$$

The electrolyte volume fraction is calculated as

$$\epsilon^t_{e(n,p)} = 1 - \epsilon^t_s - \epsilon_f$$

2.8. Calculation of surface area per unit volume

The inter-facial surface area to volume ratio for a particle with the new radius $\Lambda^t_{n,p}$ and new volume fraction ϵ_s is calculated by the following equation

$$a_{n,p} = 3\epsilon^t_{s(n,p)}/\Lambda^t_{n,p}$$

The above equations are coupled with the Newman model equations given in Table 3.

2.9. Model assumptions

All the P2D model assumptions are also equally applicable in this model. The model assumes that the negative electrode and positive electrode is filled with solid spherical particles of uniform dimension. The rate of change of Li^+ in the electrolyte is completely getting deposited on, or liberated from, the solid phase and the imbalance causes an increase of electrolyte density in separator region. The model has applicability for batteries made of materials with limited volume change and this model completely neglects the structural change of materials during intercalation and SEI formation. The solvent reduction reaction is only active during charging and completely absent during discharge [13]. The electrolyte concentration decreases with cycles due to the side reactions and this is deposited over the negative electrode as the SEI layer. The properties of the SEI are taken as similar to the solid particle for simple model demonstration.

3. Solution methodology and flow chart

A one-dimensional formulation is adopted in this work to model the P2D model equations. A FORTRAN program is developed and a finite volume based formulation is used to descretize the system of equations. An unconditionally-stable implicit method is adopted for time dependent calculations. The time descretization has first order accuracy. Mesh generation was done based on the initial radius and battery dimensions. The initial mass balance is established (Equations (1) and (2)) and the number of particles (Eq.

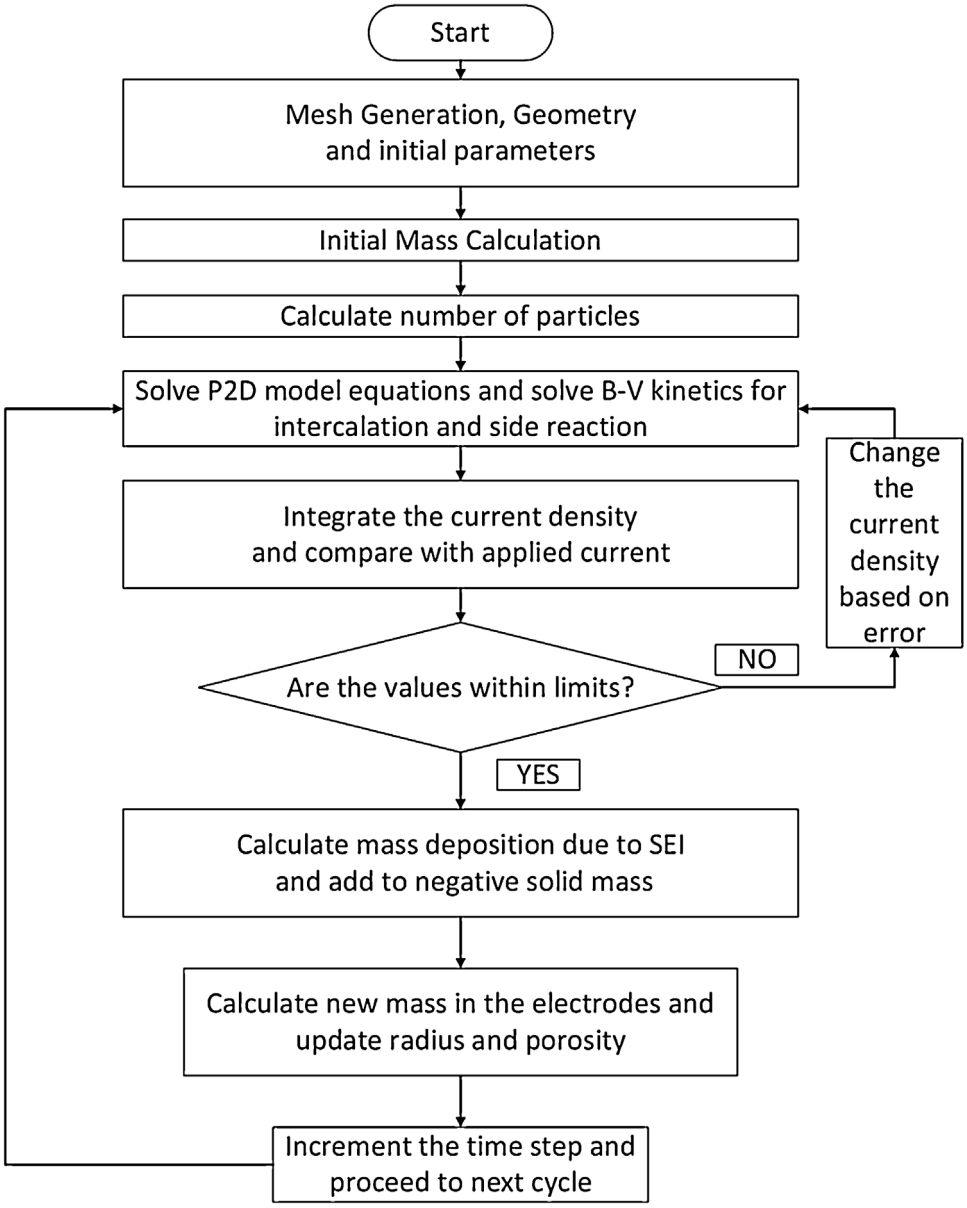

Fig. 2. FORTRAN algorithm flow chart for solving equations

(3)) is calculated based on the initial mass. The initial mass balance and the number of spherical particles remains fixed for the remaining calculations. The finite volume formulation results in a tri-diagonal form of matrix. All boundary conditions are implemented in the program in the descretization phase without any additional equations. The P2D model equations are solved sequentially using Tri-Diagonal Matrix Algorithm (TDMA). The equations are coupled together with Butler-Volmer kinetics (Table 3) and a solvent reduction side reaction (Table 3). The mass deposited on the solid particle is calculated at each time-step (Equations (5) and (8)). The total instantaneous mass of both electrodes is calculated and the model assumes that the mass is equally spread across all the particles in the electrodes. The length of the electrode remains constant, and the volume fraction changes. The side reaction SEI layer grows with cycling inducing a reduction in the current density to the system of equations. The SEI reduces the overall current density and the reduction in volume average concentration in the battery is taken as the mass deposition due to the SEI. The algorithm flowchart given in Fig. 2 shows the solution sequence.

The electrochemical parameters used in this study are for $LiCoO_2$ chemistry and have been accepted widely by the electrochemical modelling community for benchmarking their results [2], [29]. The FORTRAN model has been validated with Smith and Wang [2] for electrochemical behaviour, Ramadass *et al.* [13] for ageing and SEI growth and the thermal behaviour with Cai and White [30] to ensure its accuracy. More details of the cell validation can be found in Ashwin *et al.* [7]. The basic electrochemical predictions are within $\pm 2.0 \times 10^{-3}$ V error, capacity fading is within 2% and thermal predictions are within 1% of accuracy.

4. Results and discussion

The result is divided into three subsections, the first part discusses the effect of mass deposition on geometrical parameters such as volume fraction and particle radius. The second and third subsections focus on the effect of ageing, and performance deterioration, on the mass imbalance inside the battery.

4.1. Volume fraction and radius change during cycling

Fig. 3a shows the particle radius change at the negative and positive electrode for the first cycle of the battery. It is evident from the figure that the radius of the negative electrode increases during charging while it decreases during discharge. This is termed as "cyclic change" in the coming sections of this manuscript. The first response of applying an external current (charging or discharging) to a battery is the sharp increase in Lithium concentration in the electrolyte. The rate of change of solid concentration is slower due to difference in diffusion coefficient. This trend can be seen in all papers for example [1,31,21]. According to mass balance, this variation must be deposited on to the solid particles as lithium or its compound (in case of SEI). The inset of Fig. 3a shows the radius of the particle changes gradually and continuously within 50 seconds of applying an external current. The figure also shows an initial time delay of 5 seconds which indicates the delay of the ions in the battery to respond to an externally applied current. he increase in radius while charging is due to the intercalation reaction of lithium ions getting deposited as (LiC_6) causing the stoichiometry of the negative electrode to increase. The positive electrode shows an opposite trend where the radius decreases while charging and increases while discharging. Section 4.3 proves that SEI mass deposition will be high for the initial cycle. The first observable impact of SEI on the performance parameter of the battery such as voltage, will be reflected after roughly 50 cycles for example see the testing for SONY 18650 Battery [13]. This observation can vary between different types of batteries and therefore the 50 cycle limit is arbitrarly chosen. The particle radius change is decided by the total current density ($J = J_1 + J_s$), which controls the mass deposited, or liberated, on the electrodes. The intercalation current density (J_1) contributes towards a reversible radius change during charging and discharging whereas the side reaction current density (J_s) is responsible for the irreversible mass deposit which will be added to the negative electrode during each cycle as the SEI (Eq. (4)). Thus all the conventional ageing models can be used in-line with this formulation without any modification. As discussed earlier, the value of molar mass ($\hat{V}$) in Eq. (5) must be properly adjusted to capture the mass deposit due to other side reactions such as dissociation, temperature decomposition etc. in the battery [3]. This could be the reason for very small radius and volume fraction change of the order of nanometers in this study.

The irreversible SEI filling will influence the negative electrode radius as shown in Fig. 3b. The figure shows a cyclic increase and decrease of radius during charging and discharging due to the intercalation reaction (J_1) while the $\Delta\Lambda_{SEI}$ shows the irreversible radius increase of the negative electrode particle due to SEI growth after 50 charge-discharge cycles. We can see a slight decrease in the cyclic operating time of the battery which is an indication of capacity fade. The average radius change in the positive and negative electrode during charging and discharging for the first cycle is approximately zero whereas it increases to 8.3×10^{-10}cm after 50 charging and discharging cycles. Please note that the radius change is only due to lithium deposition which is very small. Similarly, Fig. 3c shows the volume fraction change in the negative electrode during charge-discharge operation. The $\Delta\epsilon_e$ shows the decrease in electrolyte volume fraction due to the filling of SEI after 50 charge-discharge cycles. Though not shown here, the electrolyte volume fraction (ϵ_e) decreases at the positive electrode while discharging and a reverse effect occurs while charging. But there is no porous filling in the positive electrode due to the absence of side reaction. The formulations presented in Eqs. (8) and (6) shows that the irreversible mass due to SEI side reaction is active only in the negative electrode whereas this is completely absent in the positive electrode. Thus the positive electrode radius and volume fraction is completely reversible during charge and discharge whereas the negative electrode radius and volume fraction increases due to side reaction deposition. The decrease in electrolyte volume fraction during charging indicates that lithium is intercalating into the electrode depositing more mass onto the spherical particles. Comparison of volume fraction after 50 charge discharge cycles with the first cycle volume fraction shows a clear decrease in ϵ_e. The solvent reduction side reaction is responsible for this irreversible filling leading to a gradual increase of particle radius and hence the volume fraction of the electrolyte decreases. This irreversible filling will flush out more electrolyte from the negative electrode. This will seriously limit the ability of the electrolyte to supply or absorb an ample amount of lithium ions to or from the solid particles, thereby amplifying the capacity fade.

The study presented in Fig. 3 brings more accuracy in calculating the volume-specific-area (a_s) available for intercalation as well as side reactions which is calculated as $3\epsilon_s/\Lambda$. A constant radius and a constant volume fraction can result in erroneous calculation of a_s especially when the SEI layer grows. The radius Λ and volume fraction ϵ in the electrodes changes due to side reaction deposits. Therefore, a_s directly controls the accuracy of all reactions including the Butler-Volmer kinetics and overall current density (J).The usual method to overcome this problem is by using empirical correlation, which can be completely avoided by the formulation presented in this paper. Moreover the volume fraction increase and radius change is now completely independent of the partial molar concentration compared to the results reported in other literatures [7,21].

4.2. Parametric studies with different particle density and molar mass

Re-visiting Eq. (6) shows that the intercalation mass deposit ($\pm\Delta M_{n,t}$) and the mass deposit due to SEI ($+\Delta M_{SEI}$) is added to the instantaneous mass $\tilde{M}_n$. Thus both intercalation mass deposit and SEI mass deposit are lumped together and the radius change is calculated using a combined density ρ_s in Eq. (10). Separating the radius change due to intercalation and the SEI is straight forward and can be incorporated in this model as follows:

The new instantaneous mass at negative electrode is given by:

$$\tilde{M}_n = Mi_{s,n} \pm \Delta M_{n,t}$$

The radius change due to intercalation reaction and the solvent reduction SEI deposit can be corrected as:

$$\Lambda^t_{n,p} = \sqrt[3]{\frac{\tilde{M}^t_{n,p}}{\frac{4}{3}\,\pi\,\rho_s\,K_{n,p}}} + \sqrt[3]{\frac{\Delta M_{SEI}}{\frac{4}{3}\,\pi\,\rho_{SEI}\,K_{n,p}}} \tag{12}$$

The reacting solid particles in the negative and positive electrode are porous and have void spaces filled with electrolyte and also the binder. Thus, assuming a pure lithium coating for the interaction deposit is an approximation to make the model simple; finding the correct density of the deposit will be challenging. The density of the intercalation deposit can be corrected according to $\rho_s = 0.5\ (\rho_s + \rho_{void})$ where ρ_{void} represents the void space density which would be equal to the electrolyte density if the void is filled by electrolyte. This correction will bring more accuracy to Eq. (10) in calculating the radius of the particle. The molar mass $\hat{V}$ in Equations (5) and (4) must be also replaced by an average molar mass to take into account the additional impurities in the mass deposit. This correction will bring more accuracy to Equations (6) and (7) in calculating the mass deposit over the particles. Usually 10% volume expansion of the electrode is observed on a graphite based electrodes. Pinson and Bazant [12] assumes a molar mass of 26 g/mol and density is 2.6 g/cm^3 for the deposit whereas this paper considers that the deposit is purely lithium with molar mass of 6 g/mol.

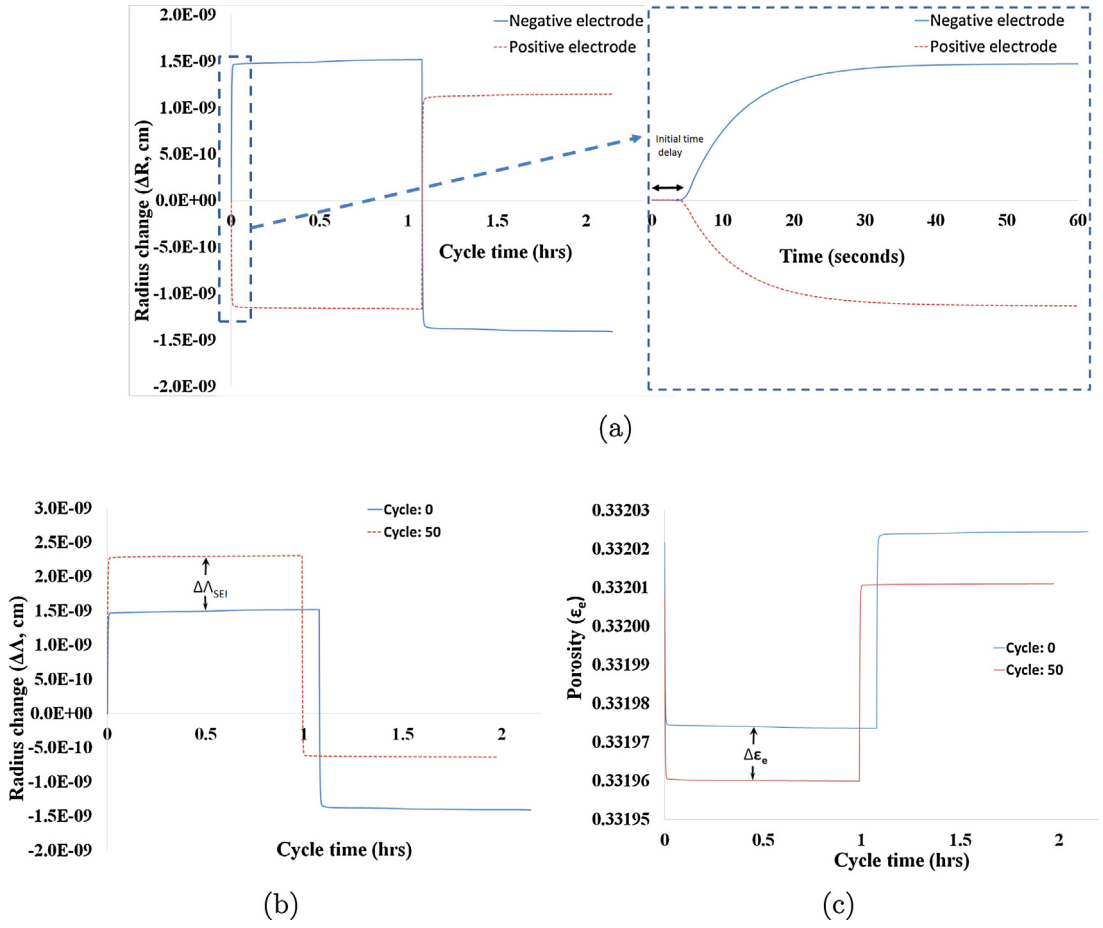

Fig. 3. Radius and volume fraction change due to lithium deposition (a) Anode and cathode radius change for the first cycle (b)Negative electrode radius change due to SEI deposition, (c) Volume fraction change after 50 cycles in the negative electrode electrolyte.

The SEI is assumed to be of a mosaic structure or a honeycomb structure; more details about this structure can be found in Peled [32] and Gauthier *et al.* [33]. Thus the density of the intercalation deposit can be corrected according to ρ_{SEI}= 0.5 (ρ_{SEI}+ρ_{void}). The mass transfer model presented in this manuscript completely neglects the honeycomb structure, or the structural deformation of SEI, and assumes that the density of SEI is similar to solid density and the SEI deposit completely covers the spherical particles without any void space. Accurate determination of SEI properties or intercalation deposits are beyond the scope of this model demonstration. However a small number of parametric studies have been performed and the results are shown in Fig. 4 to demonstrate the importance of density and molar mass on the radius change of the particle.

Fig. 4a shows the particle radius change due to intercalation reaction at the negative and positive electrode solid particle with different molar mass. The contribution from SEI is assumed negligible for the first cycle. The study shows that the radius change

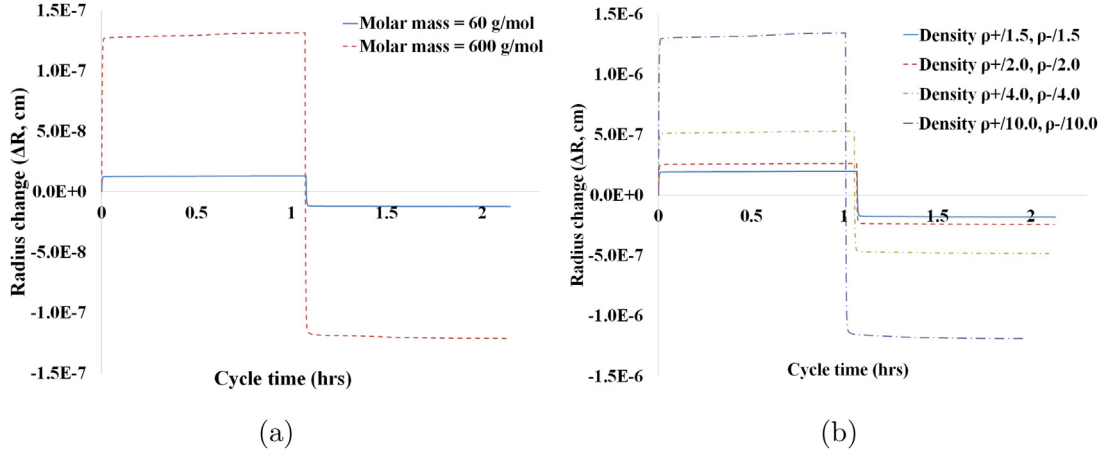

Fig. 4. Parametric studies with different molar mass and density (a) Anode and cathode radius change with different molar mass (b) Anode and cathode radius with different solid densities

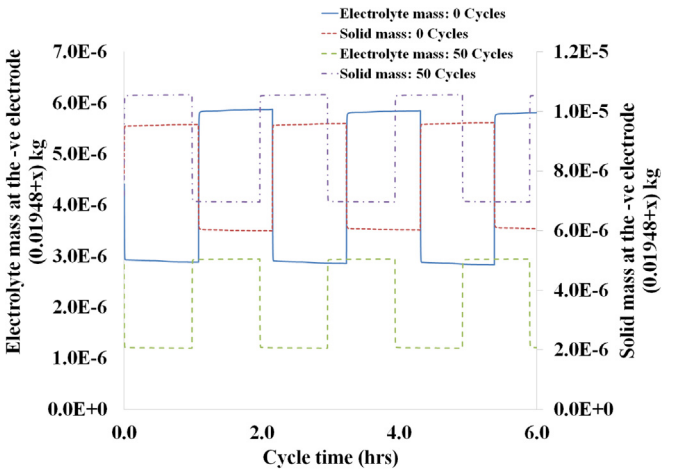

Fig. 5. Mass balance study of the battery: Solid and electrolyte mass variation with cycling

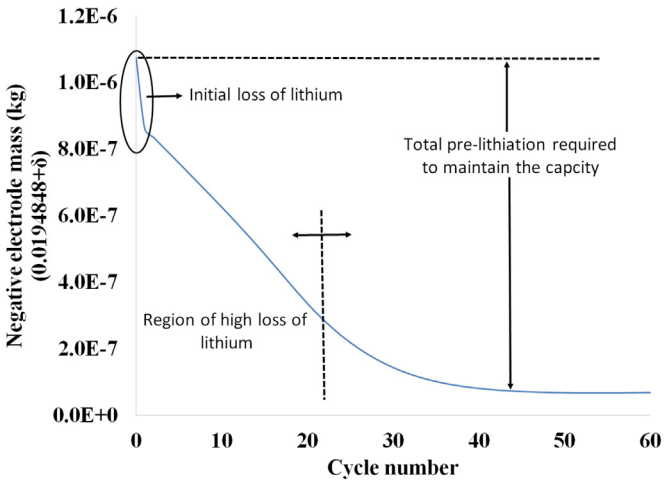

Fig. 6. Mass balance study of the battery: Loss of lithium in the negative electrode in terms of negative electrolyte mass

is almost $\pm 1.5 \times 10^{-7}$cm with molar mass of 600 g/mol compared to $\pm 1.5 \times 10^{-9}$cm reported for the molar mass of 6 g/mol. Fig. 4b shows the parametric studies by decreasing the solid particle density by a factor of 1.5, 2, 4 and 10 respectively. The present model assumes a solid particle density of 1347.3×10^{-6} kg/cm^3 on the negative electrode and 2328.5×10^{-6} kg/cm^3 on positive electrode for both intercalation and the SEI reaction. Results shows that the reduction in density results in a higher radius change and reaches almost $\pm 1.5 \times 10^{-6}$cm by reducing the density by a factor of 10.

4.3. Mass balance study during cycling

Fig. 5 shows the total solid and electrolyte mass at the negative electrode for 1C charging and discharging. There is a cyclic pattern visible for the electrolyte and solid mass with charging and discharging. This effect is governed by the intercalation reaction during charging and discharging. The charging will cause the electrolyte Li^+ ions to deposit onto the electrode forming LiC_6. This process will decrease the electrolyte mass and increase the solid mass in the negative electrode. The reverse reaction will happen in the positive electrode dissociating $LiCoO_2$ to CoO_2 thereby liberating Li^+ ions. The chemistry and the reactions presented in this work is only indicative and the framework is common for battery materials such as LTO with very limited volume change. A snapshot of electrolyte mass and solid mass after 50 cycles shows that the average electrolyte mass has decreased and average solid mass has increased. This indicates the loss of lithium due to solvent reduction side reactions contributing to SEI growth. The loss of electrolyte mass will affect the ability of the battery to transfer the Li^+ ions across the electrodes and limits the capacity of the battery. The magnitudes for electrolyte mass and solid mass is different due to the difference in density. Fig. 6 shows the negative electrode electrolyte mass which gives a possible indication of the loss of lithium from the negative electrode during cycling. The initial loss of lithium at the negative electrode is very high due to the unprotected electrodes being exposed to the reaction with electrolyte. This observation can lead to the conclusion that initial SEI formation can protect the battery from loss of lithium [3]. The loss of lithium decreases and reaches a constant value after 40 cycles, in this case. A mathematical integral of the curve presented in Fig. 6 can calculate the total lithium loss in the electrolyte up to certain cycles number of interest. This otherwise gives the pre-lithiation required for the battery.

Figs. 5 and 6 quantifies the mass and mass transfer to and from the electrodes for the first time using a full P2D model. The loss of lithium due to unprotected electrodes can be quantified in this model in terms of mass loss. The SEI will subsequently protect the electrodes after the first several cycles which limits the heavy loss of lithium even though this adds additional resistance, more details can be found in Peled [32] and Fong *et al.* [34]. Thus the loss of lithium calculated from this model (Fig. 6) is very useful for quantifying the amount of excess lithium to be added so that the battery will work effectively. This model is helpful in predicting the amount of lithium deposited on the electrodes under different operating conditions.

4.4. Effect of exchange current density on the mass balance of the battery

Fig. 7 shows the effect of solvent reduction (ageing) reaction on the density of the electrolyte in the battery. The density variation of the electrolyte is limited to the separator region and calculated using Eq. (9). The analysis use two exchange current densities, $i_{os} = 1.5 \times 10^{-12}$ and $i_{os} = 5.0 \times 10^{-10}$ which is chosen arbitrary to simulate different side reactions. A similar parametric study can be found in Ashwin *et al.* [7] and Ramadass *et al.* [13]. A higher exchange current density accelerates the solvent reduction side reaction, resulting in deposition of higher SEI mass on the particles. The first cycle shows a sharp drop in density indicating that

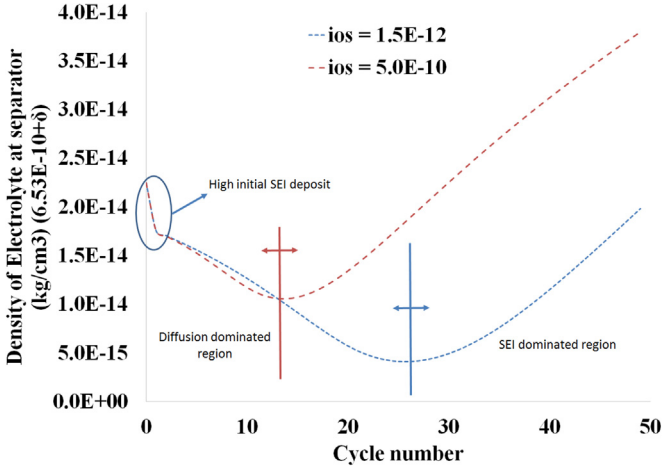

Fig. 7. Effect of ageing reaction on the performance of battery: Density variation in the separator

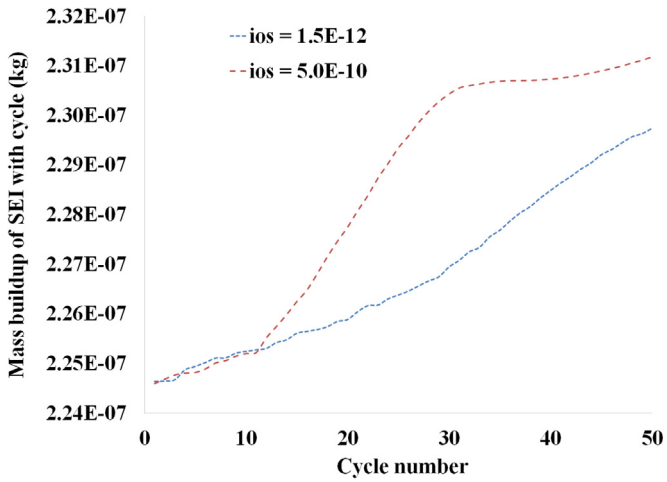

Fig. 8. Effect of ageing reaction on the performance of battery: Total mass of SEI over cycles

the lithium deposit is very heavy on an un-protected electrode and moreover, high mass of lithium is removed from the electrolyte. This removal of ions results in mass loss and sharp decrease in density of the electrolyte.

For the $i_{os} = 1.5 \times 10^{-12}$ case, the first 27 cycles shows a decrease in density whereas the $i_{os} = 5.0 \times 10^{-10}$ case shows the same trend after 13 cycles. This indicates that, up to 13 and 27 cycles for the respective cases, lesser pore filling due to SEI, and the solid mass (ions) liberated from one electrode is able to get into the other electrode easily. Thus unrestricted ion-diffusion is dominating in this region. The shape of the curve may vary with different batteries and also with the property of the electrolyte. We can observe a gradual increase in electrolyte density after 27 cycles for the $i_{os} = 1.5 \times 10^{-12}$ cases and 13 cycle for the $i_{os} = 5.0 \times 10^{-10}$ case. After these cycles, the SEI grows and the ion diffusion is more restricted which creates an imbalance in the solid mass getting deposited thereby increasing the electrolyte density. This density variation can happen in the entire electrolyte, however, in this model, is limited only to the separator region and also this is a qualitative estimation of the density variation since other side reactions can actively contribute to the contamination which is neglected in this analysis. Higher density is an indication of the higher contamination of the electrolyte due to higher degradation reactions inside the battery. Interestingly, the initial loss of lithium or the density decrease due to initial SEI deposit is same for both exchange current densities. Thus, for the first cycle, the SEI mass deposit is independent of other factors, assuming that the temperature is constant. Moreover, the initial mass deposit mostly depends only on the property of the electrolyte and the electrode. It has been already proven that the subsequent SEI build up and the ageing side reaction is influenced by factors like temperature, State of Charge (SoC), over potential etc. For more details about the SEI growth with different operating condition can be found in Ashwin *et al.* [7]. Fig. 8 shows the mass of SEI layer buildup with cycling. The higher side reaction exchange current density ($i_{os} = 5.0 \times 10^{-10}$) shows higher degradation and more mass deposition on the SEI layer. The initial mass deposit over an unprotected anode is nearly 2.25×10^{-7} kg which is very large compared to the subsequent mass deposits for each cycle. For the case with higher exchange current density, the diffusion process dominates only up to 13 cycles as shown in Fig. 7 and thereafter the SEI resistance increases. A higher mass deposition due to the SEI can be seen from Fig. 8 and its effect can be seen in Fig. 7 as the increase in contamination of the electrolyte. Thus, both Figs. 7 and 8 are interlinked; a higher exchange current density makes the electrolyte more viscous as well as depositing higher mass on SEI [3]. A similar observation can be made for the lower exchange current density ($i_{os} = 1.5 \times 10^{-12}$).

Figs. 7 and 8 indicate the results of an increased exchange current density on density and mass of the SEI. Peled *et al.* [35] suggests that 47.5 % of the SEI on soft carbon comes from the salt. It has been proved that almost 8% of the loss occur during first few cycles. Also the SEI composition depends both on the electrolyte and on the substrate and the greater thickness of the SEI on hard carbon is explained by the accumulation of electrolyte-reduction products in surface voids [35]. Adverse operating conditions such as temperature, deep discharge and over charge can possibly increase the exchange current density of the battery [13,3], but this does not influence the initial mass deposit on an unprotected anode. The density variation is an indication of the contamination of the battery due to side reactions. Thus the density variation and the amount of mass deposited over the SEI is quantified for the first time with the help of this P2D model. After a certain amount of mass deposition, the particles are more liable for cracking. More details can be found in Doron *et al.* [36].

5. Potential applications of this model and discussions

Subsection 4.1 of this manuscript quantifies the radius change and volume fraction change from fundamental electrochemical equations using the framework of a P2D model compared to the work done previously [7,8,21], this is a better approach than using partial molar concentration to calculate volume fraction variation and this modelling converts the framework of an open system battery volume fraction calculation to a closed system framework [15]. Moreover, the volume fraction variation is more critical in batteries where the volume expansion is larger, for example Silicon anode. We can completely avoid using empherical correlations and assumptions in this modelling approach compared to [5,6,19]. Subsection 4.3 quantifies the mass deposited on pores due to SEI and the corresponding stress development can be calculated. This study can possibly predict the possibility of particle cracking and more details can be seen in Garrick *et al.* [24]. Another approach is to use the model with a fixed volume fraction and then model the change in length. This is more useful for the stress development calculation since it accounts for the volumetric expansion, leading to destruction of the cell. However this methodology is not attempted since it is beyond the scope of this paper. Subsection 4.4 quantifies the lithium loss on an un-protected anode and helps in deciding the pre-lithiation required to maintain battery performance.

Fundamental mass conservation is the only extra assumption used in this model other than P2D model assumptions and hence this is applicable for all models which calculate lithium concentration in the electrolyte [37]. The same model can be extended for conditions which slow down the intercalation of lithium into the electrodes such as low temperature, high SoC and high current which generally favours lithium plating. More details can be found in Mathias *et al.* [38].

6. Conclusion

A novel mass balance based model has been developed to predict the particle radius change and volume fraction variation due to Lithium deposition. This manuscript quantifies the radius change and volume fraction change from fundamental electrochemical equations using the framework of a P2D model. The governing equations listed in this paper are based on the current knowledge available and the equations must be modified, once the mathematical treatment is available. It is still unclear at this moment how different ageing mechanisms like particle cracking, SEI dissociation, SEI dissolution etc, will affect the mass deposit. The structural

composition of SEI and the resulting effect on SEI molar mass and SEI density is also unclear. The formulation presented in this manuscript adds the capability to transform the conventional ageing models to a mass deposition model by reducing the number of electrochemical parameters. Therefore the model is capable of predicting the irreversible mass deposition due to SEI growth and reversible volume fraction variation in each cycle from fundamental electrochemistry. The SEI is now related to pore-clogging as well as internal resistance increase. This model can quantify the loss on an un-protected anode and helps in deciding the pre-lithiation required to maintain battery performance. The mass deposited on the SEI can be taken as a qualitative indication of the stress development. Operating the battery at higher ageing exchange current density shows more denser products in the separator region indicating that the performance of the battery is deteriorating.

Acknowledgements

This work was funded by the Innovate UK through the WMG centre High Value Manufacturing (HVM) Catapult in collaboration with Jaguar Land Rover and TATA Motors European Technical Centre. The authors thank Dr. Michael Lane, Project Engineer at Warwick Manufacturing Group and Dr. Shriram Santhanagopalan, National Renewable Energy Laboratory, US, for helpful discussions.

References

[1] M. Doyle, T.F. Fuller, J. Newman, Modeling of galvanostatic charge and discharge of the lithium/polymer/insertion cell, Journal of the Electrochemical Society 140 (6) (1993) 1526–1533.
[2] K. Smith, C.-Y. Wang, Power and thermal characterization of a lithium-ion battery pack for hybrid-electric vehicles, Journal of Power Sources 160 (1) (2006) 662–673.
[3] J. Vetter, P. Novák, M. Wagner, C. Veit, K.-C. Möller, J. Besenhard, M. Winter, M. Wohlfahrt-Mehrens, C. Vogler, A. Hammouche, Ageing mechanisms in lithium-ion batteries, Journal of power sources 147 (1) (2005) 269–281.
[4] S. Renganathan, G. Sikha, S. Santhanagopalan, R.E. White, Theoretical analysis of stresses in a lithium ion cell, Journal of The Electrochemical Society 157 (2) (2010) A155–A163.
[5] S.D. Beattie, D. Larcher, M. Morcrette, B. Simon, J.-M. Tarascon, Si electrodes for li-ion batteries-a new way to look at an old problem, Journal of The Electrochemical Society 155 (2) (2008) A158–A163.
[6] S.D. Beattie, M. Loveridge, M.J. Lain, S. Ferrari, B.J. Polzin, R. Bhagat, R. Dashwood, Understanding capacity fade in silicon based electrodes for lithium-ion batteries using three electrode cells and upper cut-off voltage studies, Journal of Power Sources 302 (2016) 426–430.
[7] T.R. Ashwin, Y.M. Chung, J. Wang, Capacity fade modelling of lithium-ion battery under cyclic loading conditions, Journal of Power Sources 328 (2016) 586–598.
[8] T.R. Ashwin, A. McGordon, P.A. Jennings, Electrochemical modelling of li-ion battery pack with constant voltage cycling, Journal of Power Sources 341 (2017) 327–339.
[9] B. Han, A. Van der Ven, D. Morgan, G. Ceder, Electrochemical modeling of intercalation processes with phase field models, Electrochimica Acta 49 (26) (2004) 4691–4699.
[10] G.K. Singh, G. Ceder, M.Z. Bazant, Intercalation dynamics in rechargeable battery materials: general theory and phase-transformation waves in lifepo 4, Electrochimica Acta 53 (26) (2008) 7599–7613.
[11] G.T. Teixidor, B. Park, P. Mukherjee, Q. Kang, M. Madou, Modeling fractal electrodes for li-ion batteries, Electrochimica Acta 54 (24) (2009) 5928–5936.
[12] M.B. Pinson, M.Z. Bazant, Theory of sei formation in rechargeable batteries: capacity fade, accelerated aging and lifetime prediction, Journal of the Electrochemical Society 160 (2) (2013) A243–A250.
[13] P. Ramadass, B. Haran, P.M. Gomadam, R. White, B.N. Popov, Development of first principles capacity fade model for li-ion cells, Journal of the Electrochemical Society 151 (2) (2004) A196–A203.
[14] E. Radvanyi, K. Van Havenbergh, W. Porcher, S. Jouanneau, J.-S. Bridel, S. Put, S. Franger, Study and modeling of the solid electrolyte interphase behavior on nano-silicon anodes by electrochemical impedance spectroscopy, Electrochimica Acta 137 (2014) 751–757.
[15] Y. Wang, Modeling discharge deposit formation and its effect on lithium-air battery performance, Electrochimica Acta 75 (2012) 239–246.
[16] X. Gao, Z. Ma, W. Jiang, P. Zhang, Y. Wang, Y. Pan, C. Lu, Stress-strain relationships of li x sn alloys for lithium ion batteries, Journal of Power Sources 311 (2016) 21–28.
[17] H. Kim, Effects of mechanical stresses on lithium ion batteries, ProQuest, 2009.
[18] X. Li, M. Xiao, S.-Y. Choe, W.T. Joe, Modeling and analysis of lifepo 4/carbon battery considering two-phase transition during galvanostatic charging/discharging, Electrochimica Acta 155 (2015) 447–457.
[19] P. Novák, W. Scheifele, M. Winter, O. Haas, Graphite electrodes with tailored porosity for rechargeable ion-transfer batteries, Journal of power sources 68 (2) (1997) 267–270.
[20] W. Gu, C. Wang, J.W. Weidner, R.G. Jungst, G. Nagasubramanian, Computational fluid dynamics modeling of a lithium/thionyl chloride battery with electrolyte flow, Journal of The Electrochemical Society 147 (2) (2000) 427–434.
[21] G. Sikha, B.N. Popov, R.E. White, Effect of porosity on the capacity fade of a lithium-ion battery theory, Journal of The Electrochemical Society 151 (7) (2004) A1104–A1114.
[22] U. Heider, R. Oesten, M. Jungnitz, Challenge in manufacturing electrolyte solutions for lithium and lithium ion batteries quality control and minimizing contamination level, Journal of Power Sources 81 (1999) 119–122.
[23] K. Yoo, S. Banerjee, P. Dutta, Modeling of volume change phenomena in a li-air battery, Journal of Power Sources 258 (2014) 340–350.
[24] T.R. Garrick, K. Kanneganti, X. Huang, J.W. Weidner, Modeling volume change due to intercalation into porous electrodes, Journal of The Electrochemical Society 161 (8) (2014) E3297–E3301.
[25] S. Hein, A. Latz, Influence of local lithium metal deposition in 3d microstructures on local and global behavior of lithium-ion batteries, Electrochimica Acta 201 (2016) 354–365.
[26] Q. Xu, Y. Yang, H. Shao, Enhanced cycleability and dendrite-free lithium deposition by adding potassium ion to the electrolyte for lithium metal batteries, Electrochimica Acta 212 (2016) 758–766.
[27] D. Aurbach, B. Markovsky, A. Rodkin, M. Cojocaru, E. Levi, H.-J. Kim, An analysis of rechargeable lithium-ion batteries after prolonged cycling, Electrochimica Acta 47 (12) (2002) 1899–1911.
[28] J. Scheers, S. Fantini, P. Johansson, A review of electrolytes for lithium-sulphur batteries, Journal of Power Sources 255 (2014) 204–218.
[29] B. Wu, V. Yufit, M. Marinescu, G.J. Offer, R.F. Martinez-Botas, N.P. Brandon, Coupled thermal-electrochemical modelling of uneven heat generation in lithium-ion battery packs, Journal of Power Sources 243 (2013) 544–554.
[30] L. Cai, R.E. White, Mathematical modeling of a lithium ion battery with thermal effects in comsol inc. multiphysics (mp) software, Journal of Power Sources 196 (14) (2011) 5985–5989.
[31] M. Doyle, J. Newman, A.S. Gozdz, C.N. Schmutz, J.-M. Tarascon, Comparison of modeling predictions with experimental data from plastic lithium ion cells, Journal of the Electrochemical Society 143 (6) (1996) 1890–1903.
[32] E. Peled, The electrochemical behavior of alkali and alkaline earth metals in nonaqueous battery systems-the solid electrolyte interphase model, Journal of The Electrochemical Society 126 (12) (1979) 2047–2051.
[33] M. Gauthier, T.J. Carney, A. Grimaud, L. Giordano, N. Pour, H.-H. Chang, D.P. Fenning, S.F. Lux, O. Paschos, C. Bauer, et al., Electrode-electrolyte interface in li-ion batteries: Current understanding and new insights, The journal of physical chemistry letters 6 (22) (2015) 4653–4672.
[34] R. Fong, U. Von Sacken, J.R. Dahn, Studies of lithium intercalation into carbons using nonaqueous electrochemical cells, Journal of The Electrochemical Society 137 (7) (1990) 2009–2013.
[35] E. Peled, D. Golodnitsky, A. Ulus, V. Yufit, Effect of carbon substrate on sei composition and morphology, Electrochimica acta 50 (2) (2004) 391–395.
[36] D. Aurbach, E. Zinigrad, Y. Cohen, H. Teller, A short review of failure mechanisms of lithium metal and lithiated graphite anodes in liquid electrolyte solutions, Solid state ionics 148 (3) (2002) 405–416.
[37] S. Santhanagopalan, Q. Guo, R.E. White, Parameter estimation and model discrimination for a lithium-ion cell, Journal of the Electrochemical Society 154 (3) (2007) A198–A206.
[38] M. Petzl, M. Kasper, M.A. Danzer, Lithium plating in a commercial lithium-ion battery-a low-temperature aging study, Journal of Power Sources 275 (2015) 799–807.